

Major antigen-induced domain rearrangements in an antibody

Robyn L Stanfield¹, Midori Takimoto-Kamimura^{1†},
James M Rini^{1‡}, Albert T Proffy² and Ian A Wilson^{1*}

¹The Department of Molecular Biology, The Scripps Research Institute, 10666 North Torrey Pines Road, La Jolla, CA 92037, USA and ²Repligen Corporation, One Kendall Square, Building 700, Cambridge, MA 02139, USA

Background: Recent structural results have shown that antibodies use an induced fit mechanism to recognize and bind their antigens. Here we present the crystallographically determined structure of an Fab directed against an HIV-1 peptide (Fab 50.1) in the unliganded state and compare it with the peptide-bound structure. We perform a detailed analysis of the components that contribute to enhanced antigen binding and recognition.

Results: Induced fit of Fab 50.1 to its peptide antigen involves a substantial rearrangement of the third complementarity determining region loop of the heavy chain (H3), as well as a large rotation of the variable heavy (V_H) chain relative to the variable light (V_L) chain.

Analysis of other Fab structures suggests that the extent of the surface area buried at the V_L - V_H interface correlates with the ability to alter antibody quaternary structure by reorientation of the V_L - V_H domains.

Conclusion: Fab 50.1 exhibits the largest conformational changes yet observed in a single antibody. These can be attributed to the flexibility of the variable region. Comparisons of new data with previous examples lend to the general conclusion that a small V_L - V_H interface, due in part to a short H3 loop, permits substantial alterations to the antigen-binding pocket. This has major implications for the prediction, engineering and design of antibody-combining sites.

Structure 15 October 1993, 1:83–93

Key words: antibody–antigen recognition, conformational change, induced fit, quaternary change

Introduction

The shape of an antibody can undergo considerable alteration to accommodate antigen binding, and this induced fit appears to be an important mechanism for antibody–antigen recognition [1–5]. The structures of five Fab or Fv fragments (B13I2 [1], D1.3 [2], BV04-01 [3], 17/9 [4], and DB3 [5]) in their free and bound forms all show conformational changes in their combining sites in response to antigen binding. These changes can occur by rearrangement of side chains [5], segmental shifts of complementarity determining region (CDR) loops [1], substantial rearrangements in CDR loops [3,4], or changes in the relative disposition of the V_L and V_H domains [2,3].

Fab molecules, which are fragments of complete antibody molecules, are composed of two polypeptide chains (light and heavy), each of which folds into two domains (variable and constant). The variable light (V_L) and variable heavy (V_H) chain domains are related by an approximate two-fold axis of symmetry, as are the constant light (C_L) and the constant heavy chain (C_H) domains. The variable and constant regions are connected by a flexible linker with the elbow angle describing the relationship between the pseudo two-fold axes of the V_L - V_H and the C_L - C_H domains. As a result of rotations about such elbow angles and changes in the relative disposition of the V_L and V_H domains, Fab molecules can experience quaternary structural

changes. In fact, elbow angles vary from 127° to 193° [6,7] and can differ even in Fab molecules within the same asymmetric unit of a crystal [8]. However, V_L - V_H differences have been seen only in comparisons of unliganded (native) *versus* antigen-bound Fab molecules [2,3]. It is useful to have multiple structures of both free and bound forms to evaluate whether conformational changes are brought about by ligand binding, crystal contacts, conformational disorder, or the general flexibility of antibody molecules.

We have now compared the structures of Fab 50.1 (an anti-HIV-1 peptide Fab) in its free and bound states, and observe in this one antibody the full range of conformational changes noted above, but with the largest magnitudes yet reported. We suggest on the basis of comparisons with other reported Fab structures, why some antibodies may be more flexible or ‘inducible’ than others.

Results

Structures of Fab 50.1 alone and complexed with peptide were determined by molecular replacement to 2.8 Å resolution [9], (M Takimoto-Kamimura & IA Wilson, unpublished data). For the complex, two copies (50.1.p1 and 50.1.p2) are present in the asymmetric unit of the crystal, and two different crystal forms

*Corresponding author. Present addresses: [†]Teijin Institute for Bio-Medical Research, Teijin Limited, 4-3-2 Asahigaoka, Hino, Tokyo 191, Japan and [‡]Department of Molecular and Medical Genetics, University of Toronto, Toronto, Ontario M5S 1A8, Canada.

exist for the unliganded antibody (50.1.n1 and 50.1.n2 crystallize in space groups P2₁2₁2₁ and I222, respectively). Both copies of each structure are described to show not only the similarities but also the differences that are due to the inherent flexibility of antibody molecules and not primarily to antigen binding. The Fab molecules were numbered according to standard convention [10] with light and heavy chains designated by L and H, respectively. (In 50.1, a deletion of residues H98–H100 results in a short H3 loop, such that residue Tyr^{H97} in 50.1 corresponds structurally to the residue preceding H101 in other Fab structures.)

Quaternary changes

The elbow angles for the two complexed molecules in the asymmetric unit differ by about 13° (163.9° and 176.5°) and illustrate the general flexibility of V–C interfaces. The unliganded 50.1 Fab elbow angles (175.6° and 173.5°) are similar to that of one of the peptide complexes. On the other hand, the relative orientations of the V_L and V_H domains consistently differ between the free and bound structures (Fig. 1). Comparisons were carried out as previously described ([11], see Materials and methods) by superimposing the corresponding V_L domains of free and bound 50.1 and then determining the rotations and translations required to superimpose their V_H domains. When the two peptide-bound V_Ls were superimposed, the rotations and translations required to superimpose their V_H domains were very small (1.1° and 0.18 Å). However, when the unliganded Fab was compared with the two complexes, the equivalent rotations and translations required for V_H superposition were substantial at 16.1°

and 2.7 Å, and 16.3° and 2.8 Å, respectively. This domain shift is by far the largest yet observed in a comparison of free and bound Fabs. Not only is there substantial V_L–V_H rotation in 50.1, but V_L and V_H move apart from each other in the peptide complex, such that there is a widening of the antigen-binding pocket in order to accommodate peptide antigen. The rotations do not correlate with any particular axis of the Fab and analysis of other free and bound Fabs also shows no systematic distribution of the rotational components (Table 1).

Tertiary changes

To determine whether any tertiary conformational changes accompany peptide binding, we superimposed the individual domains (V_L, C_L, V_H, C_{H1}) of the unliganded and complexed Fab 50.1 using framework residues (C α atoms) as defined by Kabat *et al.* [10]. The root mean square (rms) deviations show that the free and bound Fabs 50.1 differ significantly in only two regions, the CDR loops H1 and H3 (Table 2). A comparison between the unbound and peptide–complex structure shows that H3 undergoes a substantial rearrangement (average rms deviation of 2.7 Å for the C α residues), whereas CDR H1 moves in a rigid body or segmental fashion (rms deviations of about 1.3 Å).

This large H3 loop rearrangement is illustrated in Fig. 2. The loop in the unliganded 50.1 has an unclassified multiple turn around residues 95–101, whereas Ile^{H101} and Thr^{H102} form the second and third residues of a type-VIII (α_R – β_E) turn [12]. The electron density for the top of the loop is weak, especially around residue Glu^{H95}. The loop in the 50.1 peptide complex has a type-II (β_P – γ) turn around residues Glu^{H95} and Gly^{H96}

Table 1. Pairwise comparisons of V_L–V_H domain dispositions for free and antigen-bound Fabs.

Fab	Rotation (°)	Translation (Å)	ψ (°)	θ (°)	ϕ (°)
50.1.p1–50.1.p2	1.10	0.24	0.94	0.27	-0.21
50.1.n1–50.1.n2	1.68	0.21	-0.04	1.66	0.28
50.1.p1–50.1.n1	16.07	2.65	7.16	-13.95	2.82
50.1.p2–50.1.n1	16.29	2.84	8.27	-13.66	2.42
50.1.p1–50.1.n2	14.81	2.67	7.14	-12.35	3.32
50.1.p2–50.1.n2	15.05	2.85	8.24	-12.05	2.95
B13I2.n1–B13I2.n2	0.72	0.19	0.57	-0.40	-0.15
B13I2.n1–B13I2.p	2.93	0.60	0.33	-0.55	-2.86
B13I2.n2–B13I2.p	2.70	0.75	-0.25	-0.23	-2.68
BV04.nat–BV04.dna	7.47	0.74	3.99	6.08	-1.54
409.5.3.nat–409.5.3.fab	7.72	1.38	4.01	-5.07	4.06
17/9.nl–17/9.n2	1.92	0.46	-1.36	0.99	-0.93
17/9.n1–17/9.p1	4.21	1.03	-2.78	2.26	-2.27
17/9.n1–17/9.p2	4.05	1.07	-2.30	-0.28	-3.32
17/9.n1–17/9.p3	4.15	1.10	-1.91	-0.97	-3.54
17/9.n2–17/9.p1	2.31	0.58	-1.39	1.32	-1.28
17/9.n2–17/9.p2	2.87	0.68	-0.93	-1.21	-2.42
17/9.n2–17/9.p3	3.32	0.76	-0.54	-1.90	-2.66

The Fabs are 50.1 [9] (M Takimoto-Kamimura & IA Wilson, unpublished data), B13I2 [1], 17/9 [4], BV04 [3] and 409.5.3 (N Ban, *et al.*, & A McPherson, abstract PK07, Annual Meeting of the American Crystallographic Association, Albuquerque, New Mexico, 1993). The large changes seen for the 50.1 free versus bound structures are highlighted in bold type. For further details, see Materials and methods.

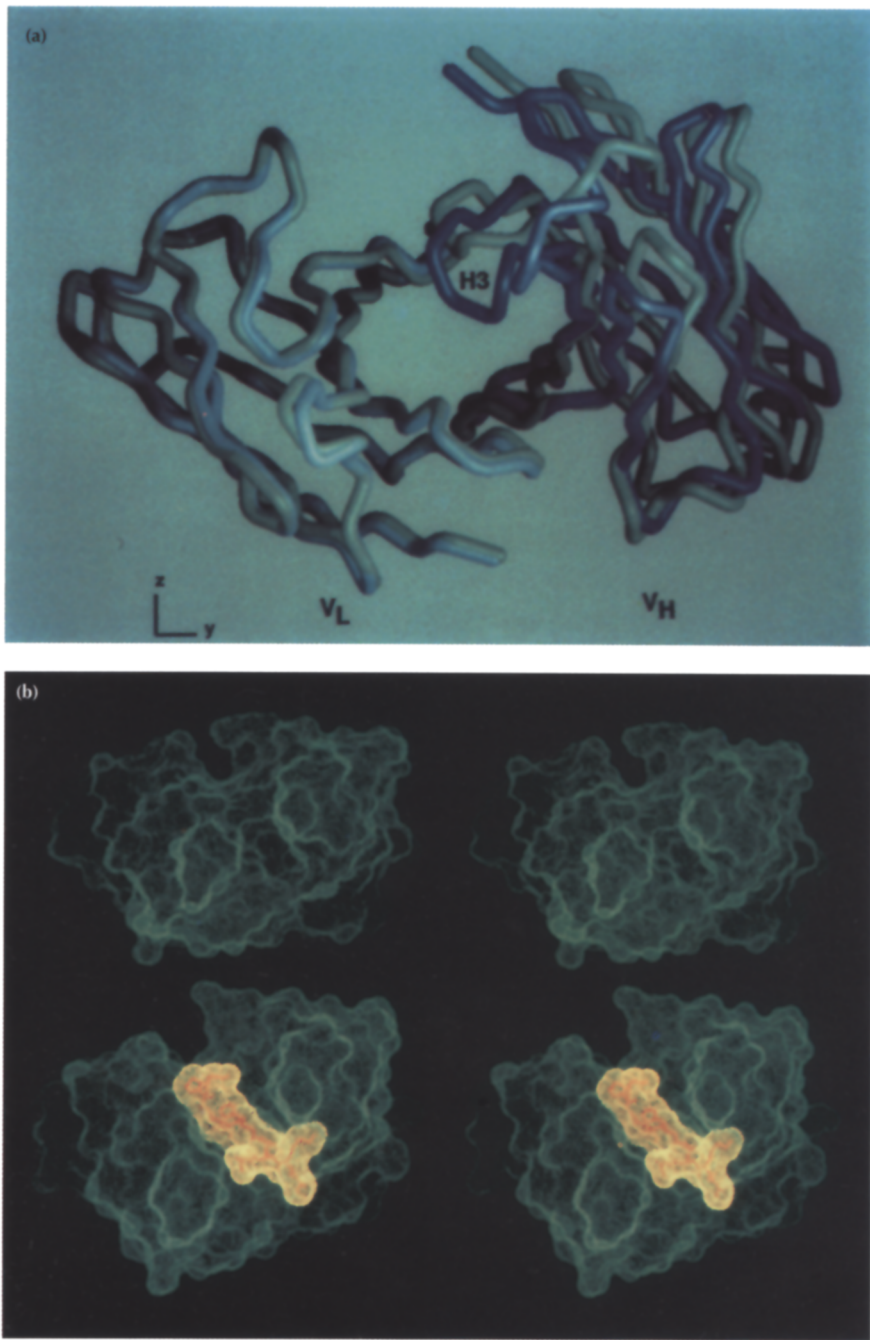


Fig. 1. (a) Superposition of Fab 50.1 unliganded and peptide-bound structures. 50.1.n1 and 50.1.p1 were superimposed using the C_α atoms of the framework residues [10] of the V_L domain. The V_L domains are on the left. The unliganded Fab is shown in blue and the antigen-bound Fab is shown in green. The rotation required to then superimpose the V_H domains is about 16° (7.2° about the x-axis, -14.0° about the y-axis and 2.8° about the z-axis; see Materials and methods for explanation of coordinate system). A rotation around the y-axis would correspond to a rotation around the elbow axis. This view is down the approximate two-fold rotation axis relating V_L to V_H. Figs. 1a, 2, 3 and 4 were calculated with the program MCS [50]. (b) Comparison of the combining sites of the unliganded and liganded forms of Fab 50.1. The solvent accessible surfaces were calculated with the program INSIGHT (Biosym Technologies) using a probe radius of 1.7 Å. The binding pocket of unliganded 50.1 (50.1.n1) is shown on top and Fab 50.1 with peptide-bound (50.1.p1) on the bottom. The antigen-binding pocket of the liganded Fab is wider and deeper than that of the unliganded Fab. This difference in size and shape of the binding pocket is created by a combination of tertiary (H1 and H3 loop movements) and quaternary conformational changes (V_L-V_H rotation). The bound peptide is shown in red and its solvent accessible surface in yellow.

and maintains the type-VIII turn between residues 101 and 102. Average main-chain rms deviations range up to 4.9 Å for Gly^{H96} and average side-chain rms deviations are as large as 6.3 Å for Tyr^{H97} (Table 3). The largest side-chain atomic deviation is at the O_η atom of Tyr^{H97}, which differs in position by about 10 Å between the free and peptide-bound structures. These changes result in the formation of hydrogen bonds between Glu^{H95} Oε1 and the backbone N and O of Gly^{H96} to the bound peptide, while H3 residues Tyr^{H97} and Ile^{H101} are in van der Waals contact with the peptide [9]. In its unliganded conformation, the H3 loop sterically blocks peptide access, so the H3 rearrangement appears to be necessary for binding of antigen.

The reasons for the observed H1 movement are not so clear. The H1 loop is not in contact with peptide in either complexed structure, so the loop movement does not result from direct interaction with antigen. Rearrangement of the H3 loop does not appear to cause this movement, because, although some contacts between the H1 and H3 loops change upon peptide binding, these contacts are not in an area of the H1 loop where movement takes place. Furthermore, the H1 loop is not involved in the V_L-V_H interface, so changes at the interface should not be responsible for H1 loop differences. Crystal packing forces can probably also be eliminated, as the H1 loops from each molecule are in different packing environments. (In 50.1.p1, N

Table 2. Comparison of the free and bound CDR loops.

	L1	L2	L3	V _L	C _L	H1	H2	H3	V _H	C _{H1}	C _{H1} *
50.1.p1 versus 50.1.p2	0.37	0.42	0.37	0.41	0.51	0.31	0.48	0.30	0.45	0.78	0.57
50.1.n1 versus 50.1.n2	0.56	0.34	0.34	0.38	0.41	0.32	0.36	0.46	0.38	0.84	0.45
50.1.p1 versus 50.1.n1	0.66	0.40	0.67	0.48	0.49	1.25	0.51	2.62	0.86	1.19	0.57
50.1.p2 versus 50.1.n1	0.64	0.41	0.53	0.47	0.47	1.42	0.53	2.74	0.86	0.99	0.54
50.1.p1 versus 50.1.n2	0.53	0.47	0.45	0.46	0.48	1.11	0.51	2.88	0.87	0.75	0.55
50.1.p2 versus 50.1.n2	0.43	0.58	0.41	0.43	0.50	1.31	0.48	2.99	0.86	0.71	0.50

The rms deviations (\AA) between $\text{C}\alpha$ atoms of the free and peptide-complexed Fab 50.1 are shown. Domains were superimposed using the program OVRLAP [36]. V_L and V_H domains were superimposed using $\text{C}\alpha$ atoms of framework residues as defined by Kabat *et al.* [10]. C_L and C_{H1} domains were superimposed using $\text{C}\alpha$ atoms of all residues. After the domains were superimposed, the rms deviations for V_L, C_L, V_H, and C_{H1} domains were calculated, including all $\text{C}\alpha$ atoms of the domain. The rms deviations for the C_{H1}* domains (lacking the disordered seven residue loop (H127–H135)) were also calculated. The rms deviations for CDR loops were calculated using the $\text{C}\alpha$ atoms of that loop. (L1: 24–34, L2: 50–56, L3: 89–97, H1: 31–35B, H2: 50–65, H3: 95–102). Significant deviations are shown in bold type.

Table 3. Conformational changes in the H3 loop.

Main chain deviations						
Residue	50.1.p1 versus 50.1.p2	50.1.n1 versus 50.1.n2	50.1.p1 versus 50.1.n1	50.1.p2 versus 50.1.n1	50.1.p1 versus 50.1.n2	50.1.p2 versus 50.1.n2
Glu ^{H95}	0.52	0.57	2.42	2.46	2.84	2.90
Gly ^{H96}	0.21	0.51	4.76	4.86	5.14	5.25
Tyr ^{H97}	0.30	0.56	1.28	1.49	1.63	1.84
Ile ^{H101}	0.44	0.39	1.83	1.88	1.70	1.79
Tyr ^{H102}	0.27	0.19	0.91	1.04	0.99	1.10
Side chain deviations						
Residue	50.1.p1 versus 50.1.p2	50.1.n1 versus 50.1.n2	50.1.p1 versus 50.1.n1	50.1.p2 versus 50.1.n1	50.1.p1 versus 50.1.n2	50.1.p2 versus 50.1.n2
Glu ^{H95}	0.61	0.88	4.19	4.66	4.02	4.55
Gly ^{H96}	—	—	—	—	—	—
Tyr ^{H97}	1.73	0.68	5.95	6.27	5.48	5.78
Ile ^{H101}	0.41	0.75	3.07	3.00	3.18	3.14
Tyr ^{H102}	0.62	0.63	3.78	4.23	3.35	3.82

The average rms deviations (\AA) for main-chain and side-chain atoms of the H3 loop (residues H95–H102) between the free and peptide complexes of Fab 50.1 are shown. The V_H domains were superimposed as described in Table 2.

of Tyr^{H32} forms a hydrogen bond with Oδ1 of Asp^{L184} of a symmetry-related molecule, while in 50.1.p2, side-chain atoms from Thr^{H31} and Met^{H34} contact residues Glu^{L187}–Asn^{L190} from molecule 1.) So, it appears that the new environment created by the other conformational changes influences the location of the H1 loop. In other Fabs, individual residues outside the loops have been shown to determine loop position, but not overall conformation [13]. Other large rms differences between free and bound 50.1 are primarily caused by local disorder, such as that for heavy chain residues 129–135. This flexible loop generally has disordered electron density and high temperature factors in Fabs [1,3,4].

Changes in binding site

The large changes in the binding site are brought about by the combination of tertiary and quaternary movements. For example, residues His^{L34} and Tyr^{H97} are in van der Waals contact distance in the unliganded Fab with their rings stacked about 3.5 \AA apart.

In the peptide-bound structure, these two residues have moved about 8 \AA apart, due to a combination of the V_L–V_H separation and the H3 loop rearrangement; a leucine residue from the peptide now inserts between His^{L34} and Tyr^{H97}.

The V_L–V_H interface

We analyzed the contact surface between the light and heavy chains at the V_L–V_H interface in order to gain a better understanding of the mechanism by which the V_L and V_H domains move relative to each other. The unliganded 50.1 structure has slightly more surface area buried at the V_L–V_H interface than the two peptide complex structures (1167 \AA^2 and 1175 \AA^2 versus 1072 \AA^2 and 1063 \AA^2). More intermolecular contacts are found at the unliganded interface (73 and 87 total contacts, and 5 and 7 hydrogen bonds for 50.1.p1 and 50.1.p2 respectively) than for the complexes (41, 46 total contacts and 3, 5 hydrogen bonds). The larger number of V_L–V_H interface contacts in the unliganded structure is consistent with the closer association of the

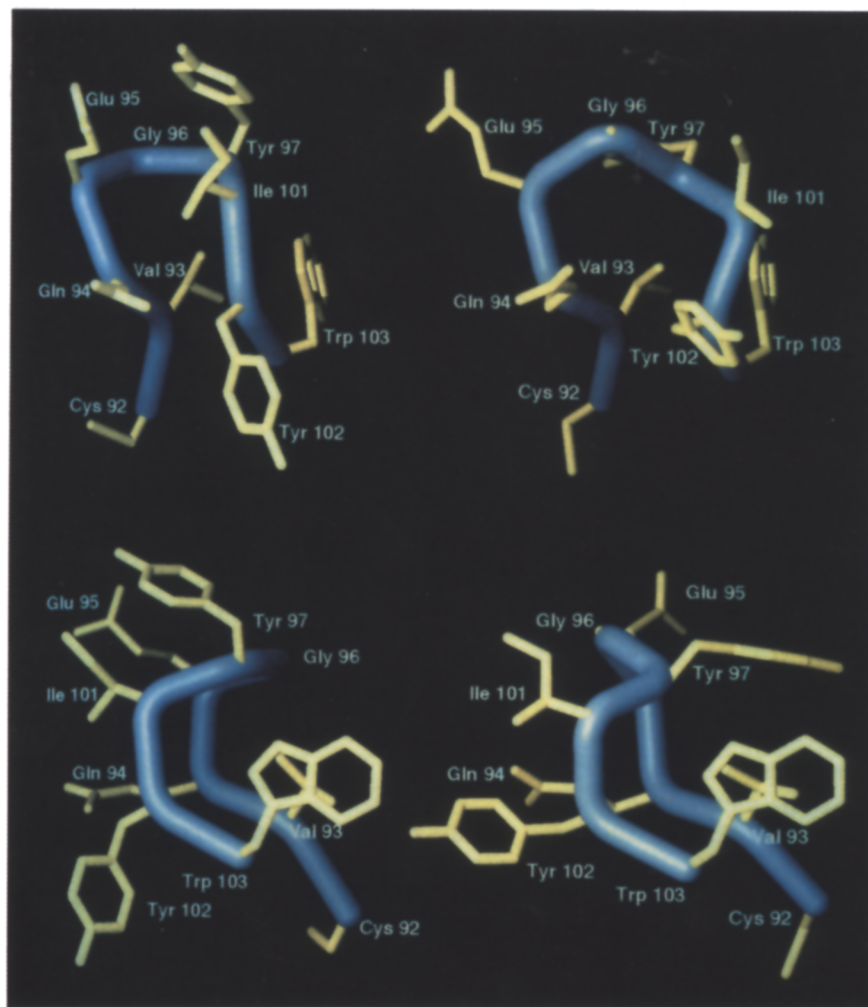


Fig. 2. Conformational change in the H3 CDR loop upon antigen binding. The unliganded H3 loop is on the left, and the H3 loop from the complex structure is on the right. Orthogonal views are shown in the top and bottom of the figure. The largest main chain movements are around residue Gly^{H96}, which has an average main chain rms deviation of approximately 4.8 Å between the free and peptide-bound structures. The largest side chain deviations are seen at residue Tyr^{H97}, which has an average side chain rms deviation of more than 6.0 Å between the free and peptide-bound structures.

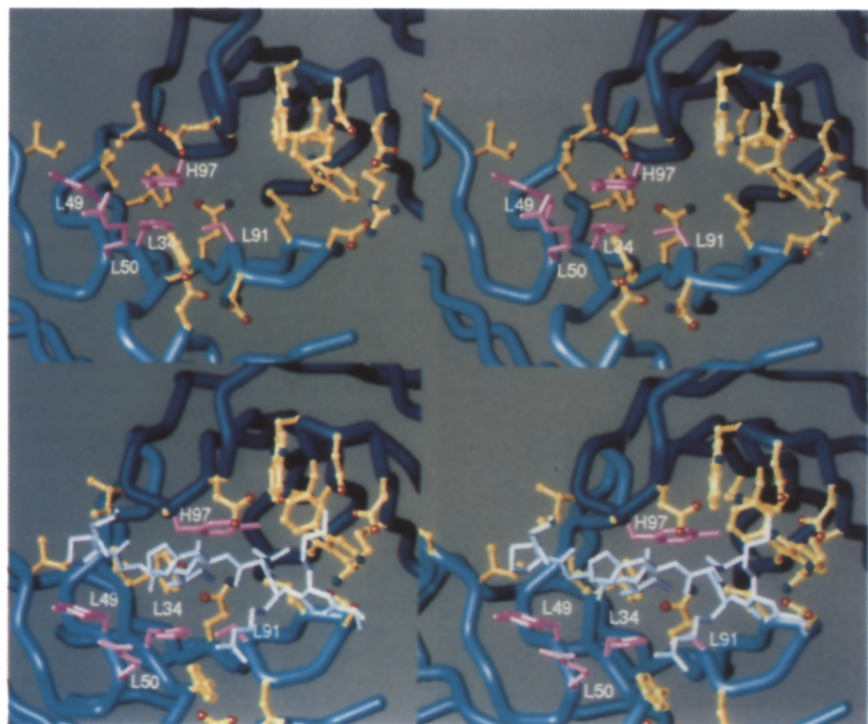


Fig. 3. Comparison of the free and peptide-bound Fab 50.1 binding sites. A stereo view of the unliganded structure is shown at the top and the peptide complex structure (with the peptide in white) is shown at the bottom. Side chains of residues contacting peptide in the complex structure are shown in yellow, and the light chain and heavy chain are light and dark blue, respectively. In the unliganded 50.1, residue Tyr^{H97} (highlighted in pink) is within van der Waals contact distance of four residues from the light chain (His^{L34}, Tyr^{L49}, Arg^{L50}, Ser^{L91}; also in pink). Notice that the rings of Tyr^{H97} and His^{L34} are packed side-by-side and over a tyrosine residue (Tyr^{L36}). In the peptide-complex structure, a combination of the H3 loop rearrangement and the V_L-V_H subunit rearrangement has widely separated these highlighted residues (by 8–11 Å), and the peptide is now bound in the cleft created between them. Peptide residue Ile^{P316} is now located over residue Tyr^{L36} and is sandwiched between Tyr^{H97} and His^{L34}.

V_L - V_H domains, indicative of a smaller 'closed' binding pocket. We should note that, although the peptide-complexed Fab has fewer self-contacts at the V_L - V_H interface, the Fab acquires an additional 60–80 contacts with the bound peptide to compensate for the loss of self-interactions [9]. Only 13 of the original 73–87 interface contacts are maintained among the four structures (Table 4). Residues making these contacts are all conserved β -sheet residues previously implicated in determining the specificity of the V_L - V_H interactions [14]. The 13 conserved contacts may serve as the pivot for the V_L - V_H rotation (Fig. 4). Residues making conserved contacts all maintain approximately the same side chain rotamer conformations in the three structures with the exception of Tyr^{H97}. Although the C β atom of Tyr^{H97} maintains a van der Waals contact with the O η atom of Tyr^{L36} in all three structures, the χ_1 torsional angle of Tyr^{H97} rotates from the *trans* conformation ($\sim 189^\circ$) in the unliganded 50.1 to an approximate gauche+ conformation ($\sim 270^\circ$) in the two 50.1 Fab-peptide complexes.

Discussion

The domain changes in the V_L - V_H interface induced by antigen provide experimental evidence for the interface adaptor hypothesis proposed by Colman [15]. The variable region is proposed to act as a flexible adaptor such that antigen can induce changes in the relative disposition of V_L - V_H and hence affect the positional relationships of the variable and light chain CDRs. This proposal was based on the variation seen in the V_L - V_H pairing of a small number of myeloma proteins which showed pairwise differences of 4–6° [11,15]. At that time no data were available for free and bound structures of the same antibody, but Colman

Table 4. Conserved contacts between V_L and V_H domains of unliganded and antigen-bound 50.1.

Contact type	V_L	V_H	Distance (Å)			
			50.1.n1	50.1.n2	50.1.p1	50.1.p2
VDW	Tyr ^{L36} O η	Tyr ^{H97} C β	3.43	3.47	3.47	3.33
HBOND	Gln ^{L38} O $\epsilon 1$	Gln ^{H39} N $\epsilon 2$	3.04	2.80	2.98	3.08
VDW	Gln ^{L38} O $\epsilon 1$	Gln ^{H39} C δ	3.63	3.72	3.64	3.66
HBOND	Gln ^{L38} N $\epsilon 2$	Gln ^{H39} O $\epsilon 1$	2.76	2.93	3.03	3.27
VDW	Pro ^{L43} C β	Tyr ^{H91} C $\epsilon 1$	3.49	3.85	4.01	3.65
VDW	Pro ^{L44} C δ	Trp ^{H103} C $\epsilon 3$	4.01	4.10	3.90	3.86
VDW	Pro ^{L44} C γ	Leu ^{H45} C $\delta 2$	3.98	3.77	3.62	3.80
VDW	Pro ^{L95} C α	Trp ^{H47} C $\zeta 3$	3.84	3.51	3.83	3.65
VDW	Pro ^{L95} C α	Trp ^{H47} C $\epsilon 3$	4.01	3.62	4.11	3.75
VDW	Pro ^{L95} C β	Trp ^{H47} C $\zeta 3$	3.78	3.71	3.93	3.90
VDW	Pro ^{L95} C β	Trp ^{H47} C $\epsilon 3$	3.85	3.62	4.09	3.82
VDW	Leu ^{L96} O	Trp ^{H47} C β	3.45	3.31	3.43	3.39
VDW	Phe ^{L98} C ζ	Ile ^{H37} C $\delta 1$	3.61	4.02	3.96	3.66

These interface contacts are maintained in the free 50.1 structure and in both molecules of the 50.1 peptide complex structure, despite the large difference in the domain dispositions between the free and antigen-bound structures. The contacts form a 'hinge' upon which the V_L and V_H domains rotate when antigen is bound. The contacts were calculated with the program CONTACSYM [37,38] with a cutoff of 3.4 Å for hydrogen bonds and salt bridges and up to 4.11 Å (depending on the atom types) for van der Waals contacts. (VDW refers to a van der Waals contact and HBOND refers to a hydrogen bond.)

suggested that the binding of antigen could cause similar changes in the quaternary structure of the variable region. The different CDRs in the myeloma proteins apparently accounted for the different V_L - V_H pairings. Hence, the large surface area buried on antigen binding was proposed to affect the interface pairing in a similar way to the CDRs themselves. It was noted earlier [14] that the β -sheet association of the variable domains is unusual (-50°) and different from the normal aligned (-30°) or orthogonal (-90°) arrangement seen for

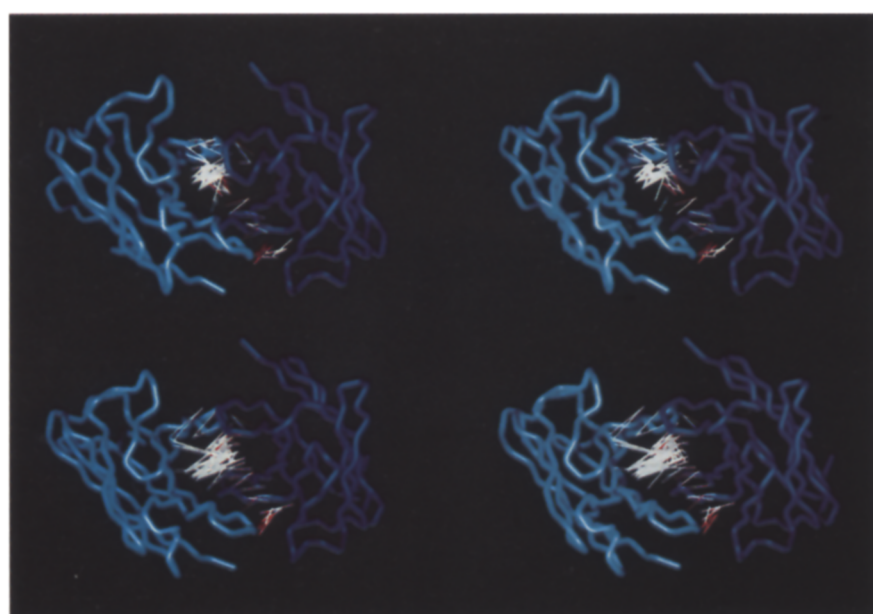


Fig. 4. Stereo view of interdomain contacts across the V_L - V_H interface of free and bound Fab 50.1. In the top half, lines have been drawn between all atoms in van der Waals contact across the 50.1.n1 V_L - V_H interface. In the bottom half, lines have been drawn between the same atoms, but in the 50.1.p1 structure. Contacts that are maintained between the unliganded and antigen-bound structures are shown as short red lines and contacts that have been changed due to atoms moving apart during the V_L - V_H rearrangement or to changes in the conformation of the H3 CDR loop are separated by long white lines. The changes in contact distances range to almost 11 Å. The light chain backbone trace is shown in light blue and the heavy chain in dark blue. For clarity, the side chains are not shown. (Contacts were calculated with the program CONTACSYM [37,38].)

other immunoglobulin domains or β -sheet proteins. This unusual pairing may in some way contribute to or favor the flexibility in domain association and may be affected by either the CDRs or by antigen.

In comparing here the V_L-V_H flexibility of the collection of free and bound Fab structures that are now available, we have made several observations. Fab 50.1 has the largest relative displacement of the V_L-V_H domains (16.3°) upon antigen binding (compared with the previous largest of 7.5° for BV04-01 [3]) and the smallest contact surface area between the V_L-V_H domains (1063 \AA^2 compared with the $1300-1675 \text{ \AA}^2$ seen previously; see Table 5). A comparison of buried surface area at the V_L-V_H interface with the relative domain movements seen upon antigen binding suggests a possible correlation. It would seem reasonable to assume that V_L-V_H domains with smaller contact surface areas find it energetically less demanding to use V_L-V_H reorientations as part of their antigen recognition mechanism. It is of interest to note that the Bence-Jones protein (light chain dimer) Loc [16] also experiences

large changes (36°) in the relative orientation of its V_L chains when crystallized under different conditions (water *versus* ammonium sulfate). Loc also has a small V_L-V_L contact area (Loc–water, 870 \AA^2 ; Loc–ammonium sulfate, 1127 \AA^2). The Loc–water structure has a concave hapten-binding pocket while the Loc–ammonium sulfate structure has a convex protrusion where the pocket is usually found.

The size of the V_L-V_H contact area also appears to be somewhat related to the size of the CDR loops, especially H3. Of 27 Fab structures examined (15 different Fabs), the contribution to the V_L-V_H interface made by framework residues ranges from $674-881 \text{ \AA}^2$, whereas the contribution to the interface from CDR loops ranges from $350-831 \text{ \AA}^2$ (Table 5). The Fab with the smallest CDR contribution to the interface is 50.1, which has a very short H3 loop (5 residues). In 50.1, the surface area buried on the Fab by binding of antigen ($\sim 530 \text{ \AA}^2$, [9]) exceeds that buried at the V_L-V_H interface by CDRs from the light and heavy chain (350 \AA^2 total, approximately half from each chain) in

Table 5. Buried surface areas at V_L-V_H interfaces of Fab molecules.

Fab	V_L-V_H interface (\AA^2)	From CDR loops (\AA^2)	From framework residues (\AA^2)	Number of residues in H3 loop	V_L-V_H rotation ($^\circ$)	Reference
50.1.p2	1063	350	712	5	16.3, 15.2	1GGI [9]
50.1.p1	1072	360	711	5	16.1, 14.8	1GGI [9]
50.1.n1	1167	493	674	5		1GGC
50.1.n2	1175	492	684	5		1GGB
NC41	1300	617	683	11		1NCA [11]
HyHEL5	1305	482	823	7		2HFL [37]
409.5.3.nat	1316	606	710	10		*
4-4-20	1375	643	732	7		4FAB [47]
BV04.nat	1387	689	698	10		[3]
BV04.dna	1404	575	829	10	7.5	[3]
B13I2.p	1409	657	751	10	2.9, 2.7	2IGF [1]
HyHEL10	1411	586	825	5		3HFM [42]
DB3.nat	1425	581	844	10		1DBA [5]
17/9.p3	1444	673	771	11	4.2, 3.3	1HIN [4]
D1.3	1453	673	780	8		1FDL [41]
17/9.p1	1455	645	809	11	4.2, 2.3	1HIN [4]
409.5.3.fab	1467	774	694	10	6.4	*
NEW	1483	650	833	9		3FAB [46]
B13I2.n1	1508	683	825	10		1IGF [1]
17/9.n2	1511	692	820	11		1HIL [4]
17/9.nl	1521	702	820	11		1HIL [4]
B13I2.n2	1537	698	839	10		1IGF [1]
17/9.p2	1545	713	831	11	4.1, 2.9	1HIM [4]
J539	1547	748	799	9		2FBJ [43]
DB3.prog	1556	676	881	10	0.0	1DBA, 1DBB [5]
KOL	1612	782	830	17		2FB4 [44]
McPC603	1675	831	844	11		1MCP [45]

Buried surface areas (\AA^2) were calculated with the programs MS [39] using a probe radius of 1.7 \AA and standard van der Waals radii [40]. The V_L-V_H rotation upon binding was calculated for Fabs where both the free (unliganded) and antigen-bound coordinates were available (Table 1). Two values for the rotation are given where there are two unliganded Fab structures available. No rotation value is given where there is only free or antigen-bound Fab, but not both. The table is ordered by size of the V_L-V_H interface. The protein data bank code and reference for each antibody is given where available. *(N Ban, et al., & A McPherson, abstract PK07, Annual Meeting of the American Crystallographic Association, Albuquerque, New Mexico, 1993.)

the ternary complex of V_L , V_H and antigen. In antibody–antigen complexes, the size of the antibody surface buried by antigen ($150\text{--}900\text{ }\text{\AA}^2$, [19,20]) varies extensively for each complex, as does the size of the interface buried by the CDRs. The Fab with the largest contribution to the interface from CDR residues ($831\text{ }\text{\AA}^2$) is McPC603, which has an 11 residue H3 loop and also the smallest surface area buried by the antigen phosphocholine ($\sim 150\text{ }\text{\AA}^2$). However, this correlation is not absolute (Table 5). For example, Fab KOL, which has a 17 residue H3 loop, has only a comparatively moderate contribution from the CDR residues to its $V_L\text{--}V_H$ interface. Nevertheless, it appears that Fab molecules with short H3 loops, and hence a small $V_L\text{--}V_H$ interface, are the most likely to use $V_L\text{--}V_H$ rotations as part of their induced fit mechanism.

The role of the H3 CDR loop in antibody sequence diversity has been recently analyzed [17]. H3 is coded by one or more of at least 10 D-minigenes and acquires further sequence and size variability by changes in the joining ends of the D and J_H genes and the addition of N and P gene sequences at the V–D and D–J junctions. An examination of the Fab sequence database established that although antibodies of different specificities may use identical light chains they rarely use identical heavy chains [17]. Diversity in heavy chains is frequently due solely to variation in the H3 loop [17]. This information, coupled with ever increasing structural evidence for the importance of the H3 loop in antigen recognition and antibody flexibility [1,3,4], implicates H3 as the dominant CDR for conferring antibody specificity via an induced fit mechanism.

In conclusion, we have seen several large conformational changes in a comparison of the free and antigen-bound 50.1 structures. In previously described structures, changes in the CDR loops between free and bound Fabs have been reported three times; as a rigid body movement ($\sim 1\text{ }\text{\AA}$ rms deviation for $C\alpha$) of H3 in B13I2 [1], as a rearrangement of H3 ($\sim 1.9\text{ }\text{\AA}$), L1 ($\sim 1.4\text{ }\text{\AA}$), and L3 ($< 1.0\text{ }\text{\AA}$) in BV04-01 [3], and as a rearrangement of H3 ($\sim 2.3\text{ }\text{\AA}$) in 17/9 [4]. $V_L\text{--}V_H$ rearrangements upon antigen binding have been seen for D1.3 [2] and for BV04-01 [3] (Table 5). In 50.1, the conformational changes include a large rearrangement of the H3 loop ($\sim 2.7\text{ }\text{\AA}$), a smaller H1 rigid body loop movement ($\sim 1.3\text{ }\text{\AA}$) and a $V_L\text{--}V_H$ rotation that is substantially larger than any seen previously. This concerted combination of large conformational changes causes the binding site in the peptide-bound Fab to broaden and change shape to create the complementarity of fit of antibody to antigen.

Although these types of changes have been documented previously, they have not been so large. However, the structural features that allow this particular Fab to undergo changes of this magnitude are likely to be present in other antibodies. The surface area analysis (Table 5) suggests that antibodies like NC41 and

HyHEL5 could utilize $V_L\text{--}V_H$ rotations in their antigen recognition mechanisms.

Biological implications

We have shown that an antibody can undergo major shape changes on binding to its antigen by changing its domain association as well as altering its local tertiary structure. The two domains of the variable region can move relative to each other by up to 16° to provide a better complementarity of fit to antigen. These and earlier results indicate that the variable regions of antibodies exhibit extreme flexibility, in sharp contrast to the rather limited range of conformational changes seen in antigens to date [18–21]. It is clear that flexibility in antibodies can be induced by antigen and this confirms earlier predictions of flexibility in $V_L\text{--}V_H$ domain association [15]. Contrary to some earlier notions [15], there is as yet no evidence that a family of conformations exists for each antibody or that crystal packing forces themselves may be sufficient to alter the domain association in antibodies as distinct from V_L dimers. Indeed, we have now seen several examples of individual free and bound antibody conformations, in which the $V_L\text{--}V_H$ pairings are similar for the free but different from the bound state. Such results are more meaningful when multiple copies of free and bound structures are available as is the case for several monoclonal antibody structures (this work and [1,2,4,5]). Small differences in the bound Fab structure have been seen for an anti-progesterone Fab' in response to the binding of a family of steroid ligands [22]. There is, however, no evidence that any signal is being transmitted to the constant domains by this mechanism. It appears that the immune system has harnessed the $V_L\text{--}V_H$ domain flexibility to add to its repertoire for adjusting fit and complementarity to antigen.

This flexibility also considerably complicates the prediction of antibody structures and their interaction with antigens [23]. Although homology modeling of antibodies [24–28] can be very effective for predicting the structure of individual V_L or V_H domains (with the exception of the H3 loop), the pairing of these two domains is difficult to predict. Furthermore, rotation of the V_H and V_L domains relative to one another can lead to large changes in the size and shape of the binding site. If our limited data are indicative of a real trend, the possibility of conformational changes will be especially likely for antibodies where the $V_L\text{--}V_H$

buried surface is small, which is usually the case when the H3 loop is short.

Our results add to earlier evidence showing that the mechanism of antibody–antigen recognition often involves induced fit [2,4,20,21] so that shape changes occur in the antibody in response to antigen. Whether antibodies that cross-react with different antigens adopt different antigen-bound structures awaits to be determined [5], although preliminary indications suggest that small but significant differences can occur in the liganded Fab when combining with different antigens [22]. Our understanding of the underlying mechanism and range of conformational changes in antibodies is still clearly limited by the availability of antibody structures and demands some caution in the prediction, design and engineering of antibody combining sites and especially in the ‘humanization’ of murine antibodies.

Materials and methods

Crystallization conditions, data collection and structure solution

Crystals of Fab 50.1 were grown in complex with peptide MP1 (*CKRIHIGPGRAYTTC*, where *C = acetamidomethylated cysteine) from 12% PEG 10 000, 0.2 M imidazole malate, 0.1 M NaCl, pH 5.5 [29]. The Fab-peptide complex crystals grow in space group P2₁ with unit cell dimensions $a = 130.3 \text{ \AA}$, $b = 52.6 \text{ \AA}$, $c = 82.0 \text{ \AA}$, $\beta = 97.5^\circ$, and with two molecules (50.1.p1, 50.1.p2) in the asymmetric unit. Data were collected with a Siemens area detector mounted on an Elliott GX-18 rotating anode generator operating at 40 mA and 55 kV. Data were reduced with the XENGEN package of programs [30] and the R_{sym} on intensity for data to 2.8 Å resolution (81% complete) was 10.0%. The structure was determined by molecular replacement using the rotation function from the MERLOT package [31], INTREF [32] for intensity-based domain refinement, and the X-PLOR transla-

tion function [33]. The structure solution is described in more detail elsewhere [9]. The current R-value for all data between 10.0–2.8 Å resolution is 0.19, with rms deviations from ideality for bond lengths and angles of 0.018 Å and 3.8°, respectively [9]. Coordinates have been deposited in the Brookhaven protein data bank (entry name 1GGI).

The unliganded Fab crystallizes in space group P2₁2₁2₁ (50.1.n1) with unit cell dimensions $a = 83.7 \text{ \AA}$, $b = 110.7 \text{ \AA}$, $c = 56.3 \text{ \AA}$ and with one molecule in the asymmetric unit. Data were collected and reduced as described for the peptide complex crystals, with an R_{sym} on intensity for data to 2.6 Å resolution of 9.6%, with data 75% complete at that resolution (84% complete to 2.8 Å resolution). The structure was determined by molecular replacement with molecule 1 (50.1.p1) of the peptide complex structure as a model. The rotation function and Patterson correlation (PC) refinement from X-PLOR [33] were used in the structure solution, followed by the modified Harada translation function (DJ Filman & JH Arévalo, unpublished data) [34]. The PC-refinement was able to correct for an elbow angle difference between the model and unknown structure of ~12° and also modify the V_L-V_H pairing by ~12°. The current R-value for all data between 10.0–2.8 Å resolution is 0.19, with rms deviations from ideality for bond lengths and angles of 0.019 Å and 4.05°. The unliganded Fab also crystallizes in space group I222 (50.1.n2) with unit cell dimensions $a = 123.1 \text{ \AA}$, $b = 119.5 \text{ \AA}$, $c = 109.5 \text{ \AA}$ and with one molecule in the asymmetric unit. Data were collected and reduced as described above, with an R_{sym} on intensities of 12.1% for data to 2.6 Å resolution. The data are 88% complete to 2.6 Å resolution (96% complete to 2.8 Å resolution). The structure was determined by molecular replacement as described above using the P2₁2₁2₁ coordinates as a model. The current R-value for all data between 10.0–2.8 Å resolution is 0.20, with rms deviations from ideality for bond lengths and angles of 0.02 Å and 3.9°. These two unliganded structures will be described elsewhere in more detail (M Takimoto-Kamimura & IA Wilson, unpublished data). Coordinates have been deposited in the Brookhaven protein data bank (entry names 1GGB and 1GGC) and a comparison of the two free (unliganded) 50.1 structures is shown in Fig. 5.

Structural analysis

In order to do pairwise comparisons (Table 1), the Fabs from the free and bound Fabs were superimposed. The variable light chain of the first Fab was first superimposed onto the variable

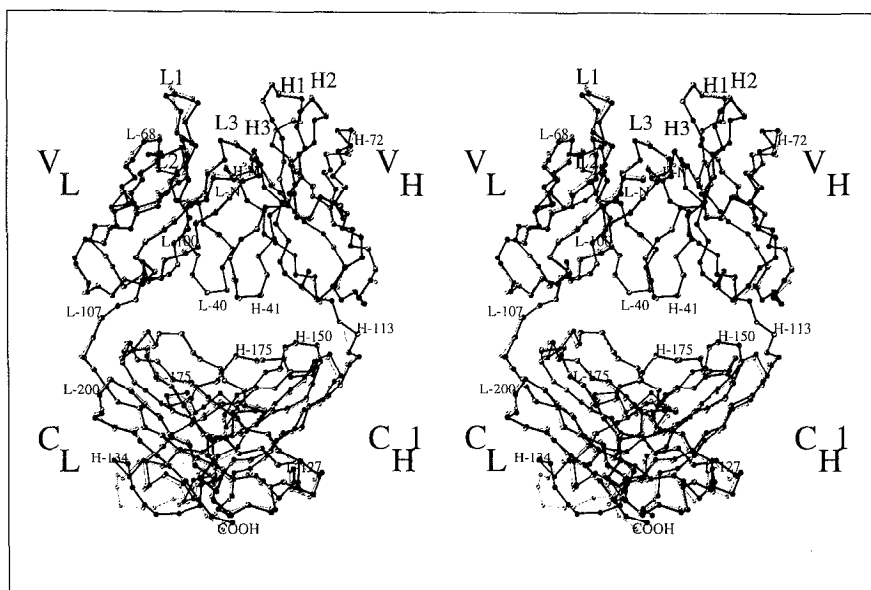


Fig. 5. Comparison of the two unliganded 50.1 structures. A Cα trace is shown with some residue numbers for reference. The CDRs are indicated by L1–3 and H1–3 as well as the domain structure by V_H, V_L, C_H1, and C_L. The 50.1 I222 structure is shown in solid lines and the P2₁2₁2₁ structure in dotted lines.

light chain of the second Fab. The same transformation was then applied to the variable heavy chain of the first Fab. The rotation and translation required to superimpose the variable heavy chains were then calculated [11]. Prior to the comparison, the reference Fab was aligned so that its pseudo two-fold axis relating the V_L and V_H domains coincided with the x-axis, and its elbow axis [line intercepting $C\alpha$ atoms of residues 107 (light chain) and 112 (heavy chain)] was in the xy-plane, almost coincident with the y-axis. The rotation required to superimpose the V_H domains was then reported as three angles ψ (the angle around the pseudo two-fold axis of the reference Fab), θ (the angle around the elbow axis of the reference Fab) and ϕ (orthogonal to ψ and θ ; Tait-Bryan angles, [35]). Domains were superimposed by $C\alpha$ atoms using the program OVRLAP [36]. Residues used for the superposition were 4–6, 20–25, 33–38, 45–48, 63–65, 70–74, 86–89, 102–104 from the light chain and 4–6, 19–24, 34–39, 46–49, 68–70, 77–81, 90–93, 107–109 from the heavy chain. Residues used for the overlap are from conserved β -sheet regions.

Multiple copies of Fabs 50.1, B13I2 and 17/9 shown in Table 1 are from more than one copy in the asymmetric unit or from more than one crystal form, or both (50.1.p1, 50.1.p2 = peptide bound 50.1 with two copies in asymmetric unit; 50.1.n1 = unliganded 50.1, space group P2₁2₁2₁; 50.1.n2 = unliganded 50.1, space group I222; B13I2.n1, B13I2.n2 = unliganded B13I2 with two copies in the asymmetric unit; B13I2.p = peptide bound; BV04.nat = unliganded BV04; BV04.dna = DNA bound; 409.5.3.nat = unliganded 409.5.3; 409.5.3.fab = 409.5.3 bound to anti-idiotope Fab; 17/9.n1, 17/9.n2 = unliganded 17/9 with two copies in asymmetric unit; 17/9.p1, 17/9.p2 = peptide bound 17/9, space group P1, with two copies in asymmetric unit; 17/9.p3 = peptide bound 17/9, space group P2₁). Comparisons of these different copies illustrate the range of rotations and translations found in any one Fab form, unliganded or complexed. An alternative way to describe the large V_L – V_H domain rearrangement is to overlap the intact variable regions using only the V_L residues and to then calculate the rms deviations between V_H domains. The rms deviations for all $C\alpha$ atoms of the V_H domain were about 4.35 Å and 4.41 Å for 50.1.n1 versus 50.1.p1 and 50.1.p2, and 0.50 Å for 50.1.p1 versus 50.1.p2.

Coordinates for Fab fragments D1.3 (1FDL, [41]) HyHEL-5 (2HFL, [37]), HyHEL-10 (3HFM, [42]), J539 (2FBJ, [43]), KOL (2FB4, [44]), McPC603 (1MCP, [45]), NEW (3FAB, [46]), and 44-20 (4FAB, [47]) were obtained from the Brookhaven protein data bank [48,49]. Coordinates for BV04 (free and DNA bound) [3], NC41 [11], and 409.5.3 (N Ban, *et al.*, & A McPherson, abstract PK07, Annual Meeting of the American Crystallographic Association, Albuquerque, New Mexico, 1993) were obtained by personal communication; coordinates for DB3 (free and progesterone-bound Fab'; 1DBA, 1DBB [5]), 17/9 (2 unliganded and 3 peptide-bound Fabs; 1HIL, 1HIM, 1HIN [4]) and B13I2 (2 unliganded and 1 peptide-bound Fabs; 1IGF, 2IGF [1]) were obtained from our own laboratory.

Acknowledgements We thank Gail Fieser for Fab production and purification, Teijin Limited for support of MT-K, and Anne Gordon for technical assistance. We also thank A Edmundson for providing BV04 coordinates, P Colman for NC41 coordinates, U Schulze-Gahmen for 17/9 coordinates, N Ban and A McPherson for the unpublished 409.5.3 coordinates and J Arévalo for DB3 coordinates, help and advice. Supported by NIH GM-46192 (IAW) and NIH training fellowship AI-07244 (RLS). RLS is a Scholar of the American Foundation for AIDS Research. This is publication #7515 MB from The Scripps Research Institute.

References

1. Stanfield, R.L., Fieser, T.M., Lerner, R.A. & Wilson, I.A. (1990). Crystal structures of an antibody bound to a peptide and its complex with peptide antigen at 2.8 Å. *Science*, **248**, 712–719.
2. Bhat, T.N., Bentley, G.A., Fischmann, T.O., Boulot, G. & Poljak, R.J. (1990). Small rearrangements in structures of Fv and Fab fragments of antibody D1.3 on antigen binding. *Nature*, **347**, 483–485.
3. Herron, J.N., *et al.*, & Edmundson, A.B. (1991). An auto-antibody to single-stranded DNA: comparison of the three-dimensional structures of the unliganded Fab and a deoxynucleotide–Fab complex. *Proteins*, **11**, 159–175.
4. Rini, J.M., Schulze-Gahmen, U. & Wilson, I.A. (1992). Structural evidence for induced fit as a mechanism for antibody–antigen recognition. *Science*, **255**, 959–965.
5. Arévalo, J.H., Stura, E.A., Taussig, M.J. & Wilson, I.A. (1993). Three-dimensional structure of an anti-steroid Fab' and progesterone–Fab' complex. *J. Mol. Biol.* **231**, 103–118.
6. Tormo, J., *et al.*, & Fita, I. (1992). Three-dimensional structure of the Fab fragment of a neutralizing antibody to human rhinovirus serotype 2. *Protein Sci.* **1**, 1154–1161.
7. Love, R.A., *et al.*, & Butler, W.F. (1993). The CHA255 antibody interacts directly with the metal in its chelate-antigen, as revealed by the 2.2 Å resolution crystal structure of the Fab'/hapten complex. *Biochemistry*, in press.
8. Prasad, L., Vandonselaar, M., Lee, J.S. & Delbaere, L.T. (1988). Structure determination of a monoclonal Fab fragment specific for histidine-containing protein of the phosphoenolpyruvate:sugar phosphotransferase system of *Escherichia coli*. *J. Biol. Chem.* **263**, 2571–2574.
9. Rini, J.M., Stanfield, R.L., Stura, E.A., Salinas, P.A., Profy, A.T. & Wilson, I.A. (1993). Crystal structure of an HIV-1 neutralizing antibody 50.1 in complex with its V3 loop peptide antigen. *Proc. Natl. Acad. Sci. USA*, **90**, 6325–6329.
10. Kabat, E.A., Wu, T.T., Reid-Miller, M., Perry, H.M. & Gottesman, K.S. (1991). *Sequences of Proteins of Immunological Interest*. (5th edn), National Institutes of Health, Bethesda, MD.
11. Colman, P.M., *et al.*, & Webster, R.G. (1987). Three-dimensional structure of a complex of antibody with influenza virus neuraminidase. *Nature*, **326**, 358–363.
12. Wilmot, C.M., & Thornton, J.M. (1988). Analysis and prediction of the different types of β -turn in proteins. *J. Mol. Biol.* **203**, 221–232.
13. Tramontano, A., Chothia, C. & Lesk, A.M. (1990). Framework residue 71 is a major determinant of the position and conformation of the second hypervariable region in the V_H domains of immunoglobulins. *J. Mol. Biol.* **215**, 175–182.
14. Chothia, C., Novotny, J., Brucolieri, R. & Karplus, M. (1985). Domain association in immunoglobulin molecules. The packing of variable domains. *J. Mol. Biol.* **186**, 651–663.
15. Colman, P.M. (1988). Structure of antibody–antigen complexes: implications for immune recognition. *Adv. Immunol.* **43**, 99–132.
16. Schiffer, M., *et al.*, & Chang, C.-H. (1989). Structure of a second crystal form of Bence-Jones protein Loc: strikingly different domain associations in two crystal forms of a single protein. *Biochemistry*, **28**, 4066–4072.
17. Kabat, E.A. & Wu, T.T. (1991). Identical V region amino acid sequences and segments of sequences in antibodies of different specificities: relative contributions of V_H and V_L genes, minigenes, and complementarity-determining regions to binding of antibody-combining sites. *J. Immunol.* **147**, 1709–1719.
18. Tulip, W.R., Varghese, J.N., Laver, W.G., Webster, R.G. & Colman, P.M. (1992). Refined crystal structure of the influenza virus N9 neuraminidase–NC41 Fab complex. *J. Mol. Biol.* **227**, 122–148.
19. Davies, D.R., Sheriff, S. & Padlan, E.A. (1988). Antibody–antigen complexes. *J. Biol. Chem.* **263**, 10541–10544.
20. Wilson, I.A. & Stanfield, R.L. (1993). Antibody–antigen interactions. *Curr. Opin. Struct. Biol.* **3**, 113–118.
21. Davies, D.R. & Padlan, E.A. (1992). Twisting into shape. *Curr. Biol.* **2**, 254–256.

22. Arévalo, J.H., Taussig, M.J. & Wilson, I.A. (1993). Molecular basis of cross-reactivity: the limits of antibody–antigen complementarity. *Nature*, in press.
23. Walls, P.H. & Sternberg, M.J. (1992). New algorithm to model protein–protein recognition based on surface complementarity. Applications to antibody–antigen docking. *J. Mol. Biol.* **228**, 277–297.
24. Chothia, C. & Lesk, A.M. (1987). Canonical structures for the hypervariable regions of immunoglobulins. *J. Mol. Biol.* **196**, 901–917.
25. Chothia, C., et al., & Poljak, R.J. (1989). Conformations of immunoglobulin hypervariable regions. *Nature* **342**, 877–883.
26. Brucolieri, R.E., Haber, E. & Novotny, J. (1988). Structure of antibody hypervariable loops reproduced by a conformational search algorithm. *Nature*, **335**, 564–568.
27. Martin, A.C.R., Cheetham, J.C. & Rees, A.R. (1989). Modeling antibody hypervariable loops: a combined algorithm. *Proc. Natl. Acad. Sci. USA*, **86**, 9268–9272.
28. Padlan, E.A. & Kabat, E.A. (1991). Modeling of antibody combining sites. *Meth. Enzymol.* **203**, 3–21.
29. Stura, E.A., et al., & Wilson, I.A. (1992). Crystallization, sequence, and preliminary crystallographic data for an anti-peptide Fab 50.1 and peptide complexes with the principal neutralizing determinant of HIV-1 gp120. *Proteins*, **14**, 499–508.
30. Howard, A.J., Gilliland, G.L., Finzel, B.C., Poulus, T.L., Ohlendorf, D.H. & Salemme, F.R. (1987). The use of an imaging proportional counter in macromolecular crystallography. *J. Appl. Crystallogr.* **20**, 383–387.
31. Fitzgerald, P.M.D. (1988). MERLOT, an integrated package of computer programs for the determination of crystal structures by molecular replacement. *J. Appl. Crystallogr.* **21**, 273–278.
32. Yeates, T.O. & Rini, J.M. (1990). Intensity-based domain refinement of oriented but unpositioned molecular replacement models. *Acta Crystallogr. A*, **46**, 352–359.
33. Brünger, A.T. (1990). *X-PLOR Manual*, Version 2.1, Yale University, New Haven, CT.
34. Harada, Y., Lifchitz, A. & Berthou, J. (1981). A translation function combining packing and diffraction information: an application to lysozyme (high-temperature form). *Acta Crystallogr. A*, **37**, 398–406.
35. Goldstein, H. (1980). *Classical Mechanics*, (2nd edn.), pp. 147–148, Addison-Wesley, Reading, MA.
36. Rossmann, M.G. & Argos, P. (1975). A comparison of the heme binding pocket in globins and cytochrome b_5 . *J. Biol. Chem.* **250**, 7525–7532.
37. Sheriff, S., et al., & Davies, D.R. (1987). Three-dimensional structure of an antibody–antigen complex. *Proc. Natl. Acad. Sci. USA*, **84**, 8075–8079.
38. Sheriff, S., Hendrickson, W.A. & Smith, J.L. (1987). Structure of myohemerythrin in the azidomet state at 1.7/1.3 Å resolution. *J. Mol. Biol.* **197**, 273–296.
39. Connolly, M.L. (1983). Analytical molecular surface calculation. *J. Appl. Crystallogr.* **16**, 548–558.
40. Gelin, B.R. & Karplus, M. (1979). Side-chain torsional potentials: effect of dipeptide, protein, and solvent environment. *Biochemistry*, **18**, 1256–1268.
41. Fischmann, T.O., et al., & Poljak, R.J. (1991). Crystallographic refinement of the three-dimensional structure of the Fab D1.3-Lysozyme complex at 2.5 Å resolution. *J. Biol. Chem.* **266**, 12915–12920.
42. Padlan, E.A., Silverton, E.W., Sheriff, S., Cohen, G.H., Smith-Gill, S.J. & Davies, D.R. (1989). Structure of an antibody–antigen complex: crystal structure of the HyHel-10 Fab–lysozyme complex. *Proc. Natl. Acad. Sci. USA*, **86**, 5938–5942.
43. Suh, S.W., et al., & Davies, D.R. (1986). The galactan-binding immunoglobulin Fab J539: an X-ray diffraction study at 2.6 Å resolution. *Proteins*, **1**, 74–80.
44. Marquart, M., Deisenhofer, J., Huber, R. & Palm, W. (1980). Crystallographic refinement and atomic models of the intact immunoglobulin Kol and its antigen-binding fragment at 0.3 nm and 0.19 nm resolution. *J. Mol. Biol.* **141**, 369–391.
45. Satow, Y., Cohen, G.H., Padlan, E.A. & Davies, D.R. (1986). The phosphorylcholine binding immunoglobulin Fab McPC603: an X-ray diffraction study at 2.7 Å. *J. Mol. Biol.* **190**, 593–604.
46. Saul, F.A., Amzel, L.M. & Poljak, R.J. (1978). Preliminary refinement and structural analysis of the Fab fragment from human immunoglobulin New at 2.0 Å resolution. *J. Biol. Chem.* **253**, 585–597.
47. Gibson, A.L., et al., & Edmundson, A.B. (1988). Differences in crystal properties and ligand affinities of an antifluorescyl Fab (4-4-20) in two solvent systems. *Proteins*, **3**, 155–160.
48. Bernstein, F.C., et al., & Tasumi, M. (1977). The protein data bank: a computer-based archival file for macromolecular structures. *J. Biol. Mol.* **112**, 535–542.
49. Abola, E.E., Bernstein, F.C., Bryant, S.H., Koetzle, T.F. & Weng, J. (1987). Protein data bank. In (Allen, F.H., Bergerhoff, G. & Sievers, R., eds) pp. 107–132, Data Commission of the International Union of Crystallography, Bonn/Cambridge/Chester.
50. Connolly, M.L. (1985). Depth-buffer algorithms for molecular modelling. *J. Mol. Graph.* **3**, 19–24.

Received: 15 July 1993; revised: 10 August 1993.

Accepted: 11 August 1993.